The Extreme Ultraviolet Emissions of W^{23+} ($4f^5$)

T Pütterich*, V. Jonauskas†, R Neu*, R Dux* and ASDEX Upgrade Team*

*Max–Planck–Institut für Plasmaphysik, EURATOM Association, D–85748 Garching, Germany
†Institute of Theoretical Physics and Astronomy of Vilnius University, A Goštauto, LT01108 Vilnius, Lithuania

Abstract. In order to comply with the special challenges (open $4f$-shell, configuration mixing) of simulating the spectrum of W^{23+} an extensive atomic model was implemented using the flexible atomic code (FAC). In detail, the basis functions from 11 configurations were used to model about 12000 levels, which give rise to roughly 60 million transitions including nearly 6 million electric and magnetic dipole transitions. A collisional radiative model has been put together which could handle the size of the input data. The modelled spectra (4–40 nm) show low sensitivity on the electron density, which validates the comparison of EBIT and tokamak spectra. The emissions between 4 and 7 nm are discussed in the context of the observations at fusion plasmas. In this range, the influence of W^{23+} is limited due to the small contribution to the measurement - however, elements of the presented modelling might explain the second, not understood spectral feature at 6 nm. Further details of the spectra are only briefly discussed as a close comparison to experimental data requires also models for the neighbouring ionisation stages. Additionally, the importance of configuration mixing becomes apparent motivating further investigations on neighbouring ionisation stages with similarly complex models.

Keywords: Tungsten Spectroscopy, Large Collisional Radiative Models, EUV Spectroscopy
PACS: 32.30.Jc,34.80.Gs,52.25.Os,52.25.Vy

INTRODUCTION

Tungsten is moving back into the focus of spectroscopy for fusion plasmas because it is used in present day tokamaks [1] as a plasma facing material in preparation of future reactor relevant devices, such as ITER [2]. There are basically two rationales why tungsten is a candidate for future fusion devices. First, it features tolerable erosion [3] such that the first wall of the reactor withstands for several years the impinging ion fluxes. Second, the retention of fuel inside of the reactor chamber is comparably small [4] and thus compatible with safety requirements. If used as plasma facing material, tungsten will be an intrinsic impurity in these plasmas as sputtering at the plasma wetted surfaces cannot be avoided. The electron temperatures of the confined plasma will span from 0.1 keV at the very edge up to 25 keV in the core. While the spectrum for tungsten ions with charges above Pd-like W^{28+} (ground state $4d^{10}$) have been subject to many theoretical and experimental investigations at fusion plasmas and electron beam ion traps (EBITs) (cf. overview in Ref.[5]), the ionisation stages with lower charge have been covered in less detail. The reason for this is the high complexity of the spectrum which is accompanied by large computational efforts for the calculation of atomic data for these ionisation stages, which exhibit an open 4f-shell leading to numerous coupling possibilities for the 4f-electrons. When considering excited states, an important group of excited levels originates from the promotion of a 4d electron to

the 4f shell, which multiplies the coupling possibilities by approximately a factor of 10. Additionally, configuration interaction and mixing plays an important role for high-Z elements. Thus, the individual wave functions are described best by including several configurations as basis function sets. As a consequence the calculations inevitably need to be huge including tens of thousands of levels and tens of millions of transitions. In the experiment, a separate consideration of ionisation stages is challenging, because the ionisation potentials of neighbouring ionisation stages are separated by only a few tens of electron volts such that even EBITs cannot prepare a single ionisation stage, further complicating the identification of spectral emissions.

In this work Sb-like W^{23+} has been tackled using the flexible atomic code (FAC) [6], while the collisional-radiative model from the ADAS project [7] was extended to be able to handle the huge input files. The spectrum of Sb-like W^{23+} is modelled in the VUV range 4-7 nm and 10-40 nm, because these wavelength ranges exhibit the strongest emissions and some experimental data are available for comparison. The range 7-10 nm neither exhibits considerable spectral radiance in the modelled spectra nor in the measurements.

The emissions in the wavelength range 4-7 nm have been investigated in detail at EBITs [8, 9], fusion experiments [10, 11, 12, 13, 14, 15, 16, 17, 18] as well as in purely theoretical studies [19, 20]. Up to now the spectral feature at 5 nm observed at tokamaks has been attributed to the emissions of Ag-like W^{27+} to Y-like W^{35+}, as lower charged ions do not exhibit a considerable abundance in the hot plasmas. Nevertheless, the suspicion is that more lowly charged ionisation stages contribute to the line of sight integrated spectra. In the present work we evaluate the importance of this contribution.

For the wavelength range 10-40 nm investigations have been performed on the spectral lines of W-ions with charges higher than W^{38+} [12, 13, 21, 14], but investigations on the emissions from ions with charges lower than W^{28+} are scarce [8, 14, 16] and open questions remain.

It should be noted that the previous investigations on the ionisation stages with an open 4f-shell are performed by tackling only a few configurations [15, 20, 16] or by applying configuration averaged calculations, which do not allow for configuration interaction. Both simplifications are known to produce unreliable predictions of the spectra for high-Z elements. In the present work, we present a calculation that includes about 12000 levels and considers roughly 60 million transitions. Due to the size of the calculation we were not able to model all ions featuring an open 4f shell, but we could elucidate the properties of the spectral emissions for one ionisation stage.

CALCULATION OF STRUCTURE AND EFFECTIVE COLLISION STRENGTHS

The energy levels, electric dipole and magnetic dipole transition probabilities and electron-impact excitation collision strengths in the distorted-wave approximation for the W^{23+} ion were obtained using FAC [6]. It realizes the Dirac-Fock-Slater approach. In the course of the calculation the configuration mixing coefficients and energy levels result from the diagonalization of the Dirac-Coulomb-Breit Hamiltonian matrix. Vacuum polarization and self energy (known as Lamb shift) treated in screened hydrogenic

approximation are included in the Hamiltonian matrix.

Figure 1 shows the diagram for energy levels used in the calculations. The present study included levels originating from the $4f^5$, $4f^45s$, $4f^45p$, $4f^45d$, $4f^45f$, $4f^35s^2$, $4f^35s5p$, $4f^35p^2$, $4f^35s5d$, $4d^94f^6$, $4d^94f^55s$ configurations. The choice of configurations is based on the highest energy level of the $4d^94f^6$ configuration which is taken as the energy of reference. All configurations which have energy levels lower than the reference one are included in the collisional radiative modelling. The difference of the highest energy level of the $4d^94f^6$ configuration and the energy of the ground level is equal to 306 eV (4 nm), i.e. the lowest limit of the shortest wavelength range (4-7 nm) studied in the present work. Because the levels of the $4f^35p^2$, $4d^94f^55s$, $4f^45f$ and $4f^35s5d$ configurations overlap with the levels of the $4d^94f^6$ configuration they were included in our modelling. However, those configurations are of odd parity and mixing with $4d^94f^6$ configuration does not take place.

The study did not take into account the $4d^94f^55p$ configuration of even parity which is closest in energy to the employed configurations. This configuration has 10934 levels and the inclusion of it would approximately double the number of transitions to be calculated. As well, many other configurations of the even parity overlap with the $4d^94f^55p$ configuration and mixing among the states of those configurations would have to be taken into account. Due to this, the rate matrix would drastically increase and the calculations would become even more challenging which is the main reason why the present work omits those configurations.

Figure 2 features the *gA* values for electric dipole transitions in the range 4-7 nm and 10-40 nm - the spectral region in-between (7-10 nm) exhibits no considerable emissions. The first interval corresponds to the transitions from the $4d^94f^6$, $4f^35s5p$, $4f^45d$ configurations to the one containing the ground state and transitions from four configurations of odd parity with the largest energies ($4f^35p^2$, $4d^94f^55s$, $4f^45f$, $4f^35s5d$) to the $4f^45s$ configuration. However, the transitions from the $4f^35s5p$ configuration to the ground configuration are not allowed in the single configuration approximation because those configurations propagate two electrons. The mixing of the former configuration with the $4f^45d$ configuration which in addition interacts with the $4d^94f^6$ configuration opens additional decay channels for the $4f^35s5p$ configuration. In a similar way, transitions from the $4f^35p^2$ to the $4f^45s$ configuration will not take place if configuration interaction is not included in the calculations.

Practically all configurations contribute to the second range of wavelengths. The total number of electric and magnetic dipole transitions in that range is equal to 4843954 compared to the 610671 transitions in the first wavelength range. However, the latter transitions are much weaker. The sum of the dipole transition probabilities is about one order of magnitude smaller for the range 10-40 nm than for transitions in the range 4-7 nm.

COLLISIONAL-RADIATIVE MODELLING

The mere size of the calculation results of FAC makes it challenging to process them in a collisional-radiative model (CRM), which was developed by the ADAS project [7] and is not optimized for computational speed. The baseline capabilities of this CRM were

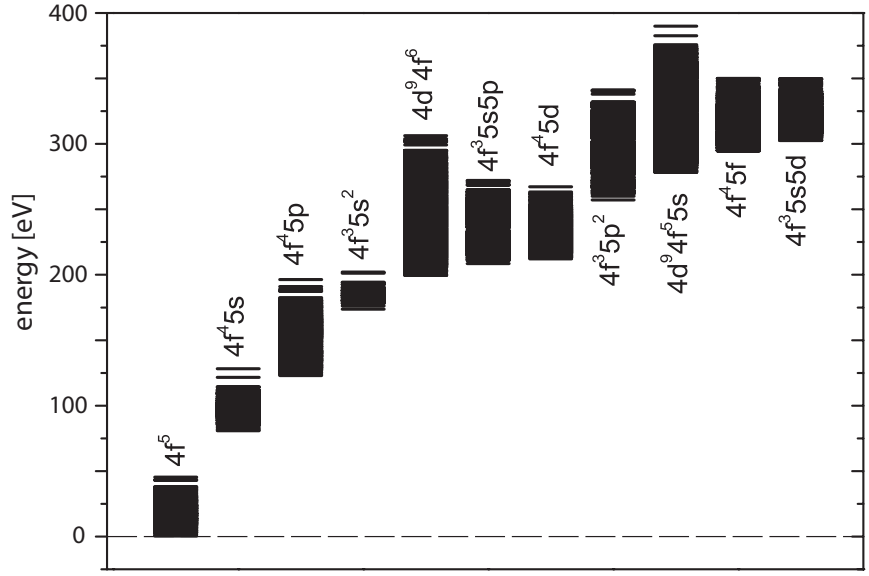

FIGURE 1. Energy levels of the first eleven configurations for W^{23+}.

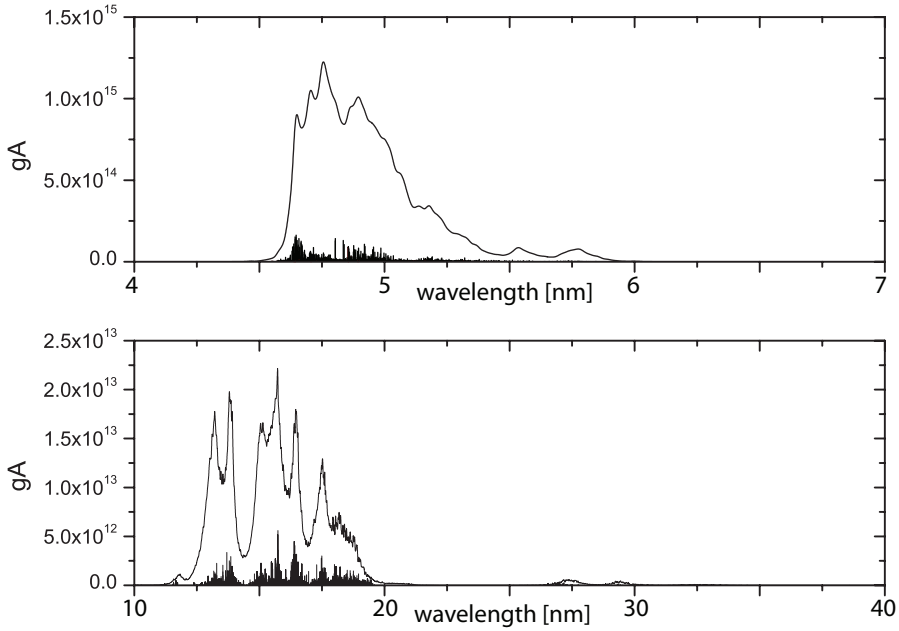

FIGURE 2. *gA* distributions for transitions in W^{23+} (bars). Lines correspond to convolved *gA* with a 0.01 nm wide Gaussian. Note the different scales.

isolated and a basic CRM optimized for speed was set up, as described below. It takes into account the excitation and de-excitation by electron impact and the spontaneous decay. The individual populations are described in a population vector $\vec{N}$ which has the size of the total number of considered levels. The population matrix $\overline{\mathrm{P}}$ is now arranged such that the multiplication $\overline{\mathrm{P}}\vec{N}$ gives the rate of change of $\vec{N}$, i.e. $d\vec{N}/dt$. Thus, the

equilibrium $d\vec{N}/dt = 0$ is found for a population vector for which $(\overline{\mathrm{E}} + \overline{\mathrm{P}})\vec{N} = \vec{N}$, where $\overline{\mathrm{E}}$ is the identity matrix. The solution of this equation is not a unique vector, as additional solutions can be produced by multiplying $\vec{N}$ with a constant, i.e. the total W-density is a free parameter. Therefore, the normalization $\Sigma_k p_k = 1$ is introduced where p_k is the population fraction in the level k.

This system of equations is solved for various combinations of electron temperature and density using the iterative biconjugate gradient method (cf. 'linbcg' in chapter 2.7 in Ref. [22]) as well as LU decomposition. Both procedures lead to the same result within the numerical accuracy. The final result is the emissivity normalized by electron and impurity ion density for each spectral line, which is called photon emissivity coefficient (PEC) and is obtained by multiplication of the relative population with the respective A-value (cf. equation below). Thus the emissivity ε_{ij} of a spectral line emitted by the decay of level i into level j is given by:

$$\varepsilon_{ij} = n_e n_{W^{23+}} p_i A_{ij} = n_e n_{W^{23+}} \mathrm{PEC}_{ij}$$

where n_e is the electron density, $n_{W^{23+}}$ the density of W^{23+} and PEC_{ij} is the PEC for the transition between the levels i and j.

COMPARISON WITH EXPERIMENTAL DATA

EUV emissions in the range 4-7 nm

In the following, the basic structure of the spectral emissions of W^{23+} and its density dependence are investigated in order to judge the degree of correspondence between spectra from EBITs and fusion plasmas. Furthermore the importance of the W^{23+} emissions in a typical spectrum from a fusion plasma, i.e. a line of sight integrated measurement across the full cross section of a plasma, will be analyzed.

In this wavelength range an intense spectral feature has been observed in various fusion experiments [10, 11, 12, 13, 14, 15, 16, 17, 18]. However, detailed comparisons between tokamak and EBIT spectra [13] reveal that a considerable fraction of the emissions observed in fusion experiments for $T_e < 2\,\mathrm{keV}$ cannot be brought into accordance neither with the EBIT observations [8] nor with modelling [14]. In figure 3, modelled spectra are presented for the electron densities 10^{17} and $10^{20}\,\mathrm{m}^{-3}$ corresponding to typical EBIT densities and tokamak densities, respectively. In both cases the electron velocity distribution is Maxwellian corresponding to 400 eV (close to maximum abundance of W^{23+}). As can be judged from the figure, the effect of electron density on the spectral emissions is rather moderate, which further motivates comparisons between EBIT and tokamak spectra.

In figure 4, the measurements of the Berlin EBIT (cf. Refs. [8, 13]) are compared to a spectrum from the tokamak ASDEX Upgrade. The latter spectrum was measured for a plasma with central plasma temperature of 2.1 keV and is presented alongside its modelling considering the ionisation stages W^{27+}-W^{35+} (blue) and W^{23+} (red) separately. All three curves have the same scale and can be compared to each other. The blue model curve reproduces the observed intensity of the tokamak spectrum if

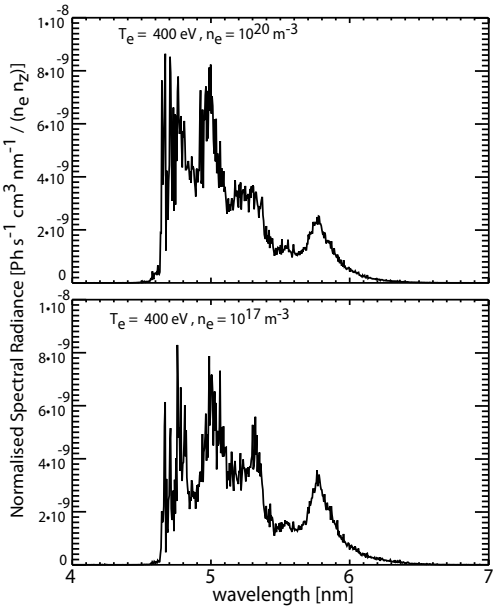

FIGURE 3. Modelled spectrum for W^{23+} at two densities, 10^{17} and $10^{20}\,m^{-3}$, for an electron temperature of 400 eV (close to the maximum abundance of W^{23+} (cf. figure 6 in [14])). The individual lines are broadened using the assumption that the electron and ion temperatures are equal. In the experiment the broadening by the instrument functions is dominant since the instrumental broadening is reported to be 0.02-0.025nm [8, 14], while at 400 eV the Doppler broadening is less than 0.0006 nm at 5 nm.

integrated over wavelength, but lacks the detailed spectral shape (for more details see [13, 14]). The EBIT investigations [8] for the ionisation stages from Ag-like W^{27+} to Y-like W^{35+} (cf. spectra in figure 4 with beam energies between 0.87 and 1.52 keV, note that for a beam energy of 1.52 keV W^{36+} may be produced, but the spectrum exhibits contributions from lower charged ionisation stages) found good agreement with the calculated atomic data which were based on the transitions between the configurations $4p^6 4d^{n-1} 4f$-$4p^6 4d^n$ (e.g. [8]) and $4p^5 4d^{n+1}$-$4p^6 4d^n$ and configuration interaction was found to play a crucial role. However, the tokamak spectrum, which is a superposition of the emissions of all ionisation states that exist along a line of sight, exhibit additional emissions at 6 nm (cf. bottom figure 4). One suspicion is that the additional radiation at 6 nm observed in fusion plasmas is caused by ionisation stages more lowly charged than Pd–like W^{28+}. The EBIT measurements in Ref. [8] with beam energies below 0.87 keV suggest that these ionisation stages exhibit emission lines in the respective wavelength range, while the structure of the EBIT spectra for these ionisation stages does not reproduce the observations from ASDEX Upgrade (cf. figure 4, bottom). The EBIT measurements for beam energies below 0.87 keV exhibit a rather smooth emission shape versus wavelength, while the modelling in the present work exhibits two clear structures for both modelled densities, i.e. one between 4.6 and 5.5 nm and the other at about 5.8 nm (cf. figure 3). The structure at 5.8 nm has a full width half maximum of about 0.2 nm. It is unclear, why the EBIT measurements are less structured than the modelling. A possible explanation could be that in the EBIT spectra more than one ionisation stage contributes and while the individual ionisation stages might exhibit quite

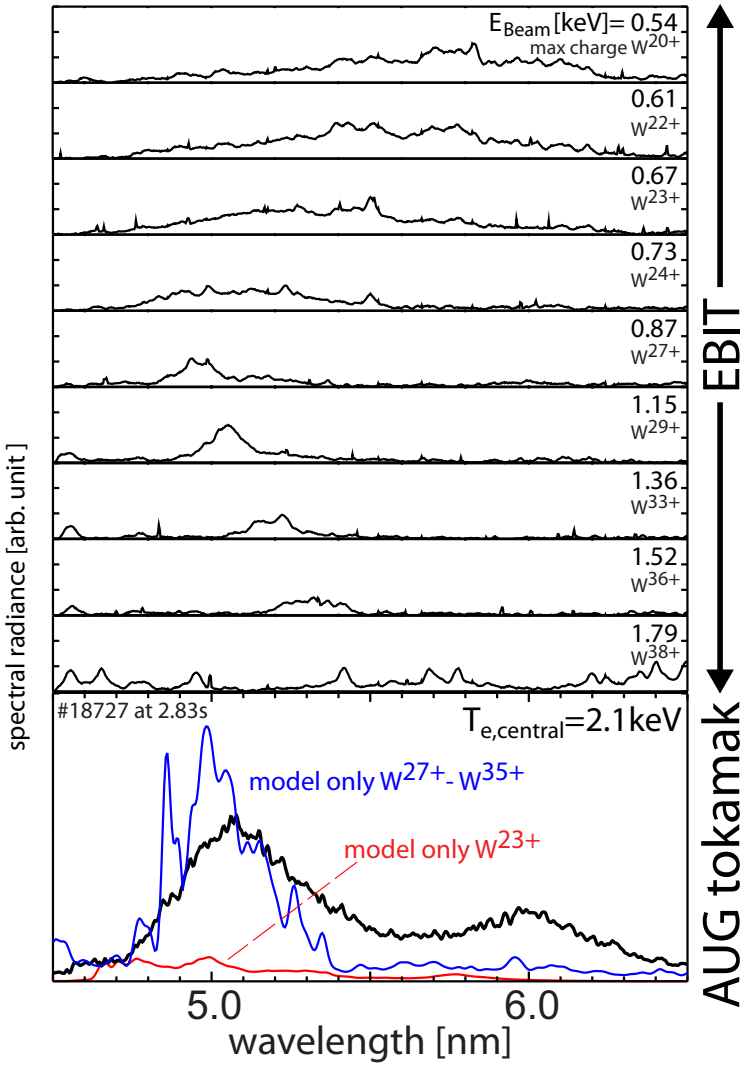

FIGURE 4. A few spectra from EBIT investigations [8] are compared to a spectrum from the tokamak ASDEX Upgrade and modelled spectra corresponding to the tokamak spectrum. The modelled spectrum for W^{23+} (red) and the modelled spectrum for W^{27+} to W^{35+} (blue) are shown on the same scale as the measurement. For the EBIT spectra the applied beam energy and the maximum obtainable charge stages (single impact ionisation) are stated using ionisation potentials from Ref. [23].

structured emissions the superposition of all the emissions look smooth. This effect is known for the tokamak spectrum, where even more charge stages contribute. Note that in none of the EBIT spectra there is an indication for a maximum at 6 nm. An alternative explanation for both observations could be additional processes, such as dielectronic recombination, which have not been included in the calculations and contribute more or less significantly to the tokamak spectrum. Further investigations on the ionisation stages around W^{23+} in similar detail are needed to clarify this question. As mentioned above the model sees no significant change of the spectrum for a change of the density. This means that spectral structures of W^{23+} as observed in EBIT measurements should

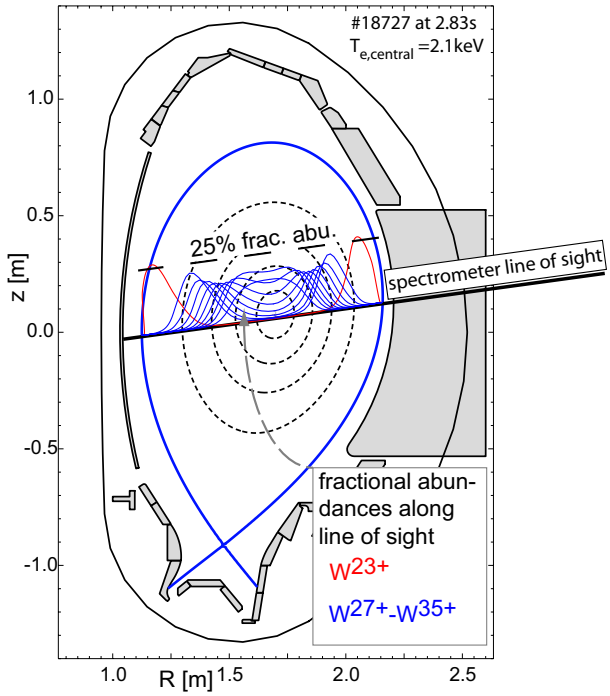

FIGURE 5. Geometry of the tokamak measurement yielding the spectrum in figure 4. The fractional abundances (from model in [14]) along the spectrometer line of sight are indicated by the blue (W^{27+} – W^{35+}) and red (W^{23+}) lines above the line of sight of the spectrometer.

look very similar to those observed in spectra from fusion plasmas.

In order to illustrate the contributions of the various ionisation stages, the fractional abundances of the relevant ionisation stages along the spectrometer's line of sight are indicated in figure 5. The fractional abundances were calculated using atomic data as derived in [14]. It should be noted that the underlying recombination rates from the average ion model (radiative + dielectronic recombination) [24, 25] have been adjusted as described in Ref. [14] such that the experimentally determined fractional abundances for several ionization stages are reproduced. No other available dataset could reproduce the experimental findings. In figure 5, W^{23+} only exists in a layer at the plasma edge and its contribution in the measured tokamak spectrum of figure 4 (red) is small, but comparable to that of one of the ionization stages of W^{27+} - W^{35+}. However, for lower charged ionisation stages the layer in which these lower charge stages exist in the plasma is even thinner and the absolute densities at the edge are smaller. Thus, it is hard to imagine that the local maximum around 6 nm results from emissions by W^{14+} to W^{27+}, i.e. ionisation stages with an open 4f-shell.

Nevertheless, the modelled data exhibits two distinct structures - one between 4.6 and 5.5 nm and one around 5.8 nm (better visible in figure 3). As the previous modelling efforts (W^{27+}–W^{35+}) for the same spectral range did not reproduce the structure of two local maxima it is worthwhile to look into the transitions that give rise to the second maximum. From earlier modellings (cf. Ref. [14]) it is derived that the transitions of the type $4p^6 4d^9 4f^{n+1}$-$4d^{10} 4f^n$ play a crucial role for these low energy/temperature emissions in

this wavelength range 4.6 and 5.5 nm. For the present modelling of W^{23+} the emissions between 4.6 and 5.5 nm correspond mainly to transitions of the type $4d^9 4f^6$-$4d^{10} 4f^5$, while many configurations are involved in the transitions between 5.7 and 5.9 nm. In descending importance the following transitions contribute to the emissions in the range 5.7 to 5.9 nm(the first type of transition contributes about 10 times more intensity than the last): $4f^4 5d$-$4f^5$ – $4d^9 4f^6$-$4d^{10} 4f^5$ – $4f^3 5s5p$-$4f^5$ – $4f^4 5f$-$4f^4 5s$ – $4d^9 4f^5 5s$-$4d^{10} 4f^4 5s$ and $4f^3 5s5d$-$4f^4 5s$. As a conclusion this means that in order to reproduce the local emission maximum at 5.8 nm a large amount of configurations need to be included in the calculation. Considering that this might have been missed out on the modelling efforts for the ionisation stages Ag-like W^{27+} up to Y-like W^{35+} these should be revised in order to possibly reproduce the emission maximum at 6 nm as observed in the tokamak spectra.

It should be noted that the identification of contributing configurations does not mean that the calculation result is the same if only these configurations are included as basis function sets. The not mentioned configurations may influence the result significantly, an effect which is attributed to configuration mixing and non-linear behaviour of collisional radiative models.

EUV emissions in the range 10-40 nm

In Ref. [14], it has been found that the spectral emissions in the wavelength range 10-40 nm originate from the edge plasma region with electron temperatures below about 1 keV. For this temperature range the ionisation stages of W up to about Pd–like W^{28+} exist in relevant abundances. From the modelling of W^{24+} to W^{26+} in Ref. [14], which was performed with a limited set of configurations, it was concluded that the W-emissions between 20 and 28 nm must originate from even more lowly charged ionisation stages. In figure 6 the modelled spectra of W^{23+} are presented for the two electron densities 10^{17} and $10^{20} m^{-3}$ in this wavelength range. Both cases are similar to a degree that again the application of EBIT findings for the interpretation of tokamak spectra seems sensible. In the calculations the emissions in the range 10-20 nm are provided by transitions of the type $4f^4 5s$-$4f^5$ – $4f^4 5p$-$4f^4 5s$ – $4f^4 5d$-$4f^4 5p$ and $4d^9 4f^6$-$4d^{10} 4f^4 5p$. In the range 28 to 32 nm transitions of the type $4f^4 5p$-$4f^4 5s$ are dominant. In Ref. [14], the modelled emissions of W^{24+} to W^{26+} correspond to the configurations $4d^{10} 4f^{n-1} 5p$-$4d^{10} 4f^{n-1} 5s$. In the present calculations the corresponding emissions in W^{23+} are also identified as important, however, additional transitions from other configurations are found to also emit considerable number of photons in this wavelength range.

SUMMARY AND CONCLUSION

An extensive atomic model for W^{23+} has been implemented using the flexible atomic code (FAC). The approximately 12000 levels have been modelled using basis functions from 11 configurations. The spectral contributions from 6 million electric and magnetic dipole transitions have been considered. Furthermore, the collision cross sections for

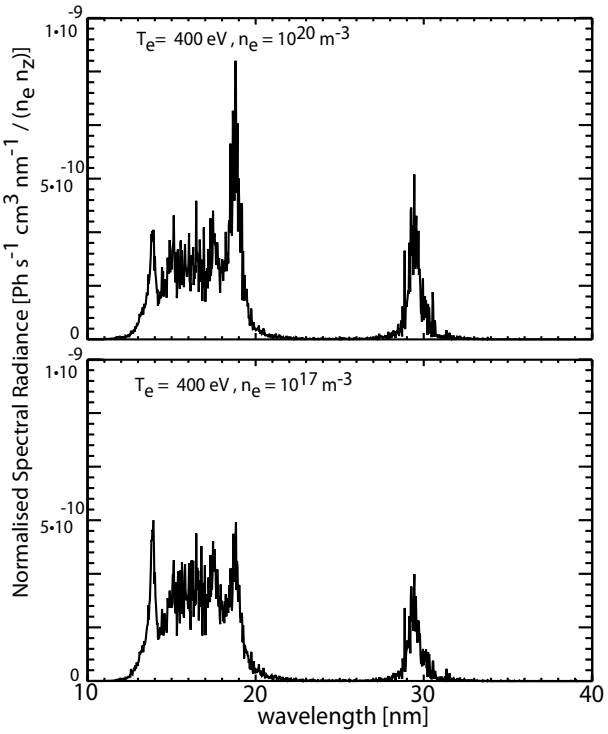

FIGURE 6. Modelled spectrum for W^{23+} at two densities, 10^{17} and $10^{20}\,m^{-3}$. Please note the different scale as compared to figure 3.

electron impact have been evaluated for roughly 60 million transitions using the distorted wave approximation. This input data was then processed with a baseline collisional radiative model that considers electron impact excitation and de-excitation as well as radiative decays by electric and magnetic dipole transitions. The resulting spectra show only a weak dependence on electron density which suggests that also for W^{23+} the spectra from EBIT devices can be used to interpret the spectra from fusion devices in order to identify the emitting ionisation stages responsible for observed spectral features. The modelled spectra exhibit strong emissions at 5 nm, which can also be reproduced by much simpler atomic models (cf. earlier work). However, for the first time the modelling provides a possible explanation of the second maximum in the spectrum at about 6 nm: while the modelled spectra exhibit this second maximum at 5.8 nm it is speculated that the spectra of higher charged ionisation stages when modelled with the same amount of detail might exhibit a similar maximum at longer wavelengths.

Additional emissions are found between 10 and 35 nm. Again simpler models have also reproduced emissions in this spectral range, however, the more complicated model (present work) demonstrates that configuration interaction and mixing is crucial. Therefore it is suggested that all the ions between W^{14+} and W^{35+} ought to be approached in similar detail as described in the present work. As computing power increases also a re-evaluation of the W^{23+} spectra should be undertaken by including the $4d^9 4f^5 5p$ configuration and by extending the optical transitions to those of quadrupole and possibly octupole type.

ACKNOWLEDGEMENT

This research was partly funded by European Social Fund under the Global Grant Measure (No.: VP1-3.1-SMM-07-K-02-015)

REFERENCES

1. R. Neu *et al.*, Plasma Phys. Control. Fusion **53**, 124040 (2011).
2. R. Pitts *et al.*, J. Nucl. Mater. **415**, S957 (2011).
3. H. Bolt *et al.*, J. Nucl. Mater. **329-333**, 66 (2004).
4. J. Roth *et al.*, J. Nucl. Mater. **390-391**, 1 (2009).
5. A. Kramida, Can. J. Phys. **89**, 551 (2011).
6. M. Gu, Astrophys. J. **582**, 1241 (2003).
7. H. P. Summers, The ADAS User Manual, version 2.6 http://adas.phys.strath.ac.uk (2004).
8. R. Radtke *et al.*, Phys. Rev. A **64**, 012720 (2001).
9. S. Utter, P. Beiersdorfer, and E. Trabert, Can. J. Phys. **80**, 1503 (2002).
10. R. Isler, R. Neidigh, and R. Cowan, Phys. Lett. **A63**, 295 (1977).
11. E. Hinnov and M. Mattioli, Phys. Lett. **A66**, 109 (1978).
12. K. Asmussen *et al.*, Nucl. Fusion **38**, 967 (1998).
13. T. Pütterich *et al.*, J. Phys. B: At. Mol. Opt. Phys. **38**, 3071 (2005).
14. T. Pütterich *et al.*, Plasma Phys. Control. Fusion **50**, 085016 (2008).
15. C. S. Harte *et al.*, J. Phys. B: At., Mol. Opt. Phys. **43**, 205004 (2010).
16. C. Suzuki *et al.*, J. Phys. B: At., Mol. Opt. Phys. **44**, 175004 (2011).
17. Y. A. Podpaly *et al.*, Can. J. Phys. **89**, 591 (2011).
18. O. Meyer *et al.*, J. Nucl. Mater. accepted (2013).
19. V. Jonauskas, S. Kucas, and R. Karazija, J. Phys. B: At., Mol. Opt. Phys. **40**, 2179 (2007).
20. D. Kilbane, J. Phys. B: At., Mol. Opt. Phys. **44**, 165006 (2011).
21. Y. Ralchenko *et al.*, J. Phys. B: At., Mol. Opt. Phys. **40**, 3861 (2007).
22. W. H. Press, S. A. Teukolsky, W. T. Vetterling, and B. P. Flannery, *Numerical recipes in C (2nd ed.): the art of scientific computing* (Cambridge University Press, New York, NY, USA, 1992).
23. A. Kramida and J. Reader, At. Data Nucl. Data Tables **92**, 457 (2006).
24. D. Post *et al.*, At. Data Nucl. Data Tables **20**, 397 (1977).
25. D. Post, J. Abdallah, R. Clark, and N. Putvinskaya, Phys. Plasmas **2**, 2328 (1995).